

# Crown Ether-Cycloparaphenylene Hybrid Multimacrocycles: From Guest Binding to Biological Application Evaluation

Yaning Hu,<sup>1</sup> Tong Li,<sup>2,3</sup> Taotao Su,<sup>1</sup> Wudi Shi,<sup>1</sup> Yabing Yu,<sup>1</sup> Beibei Li,<sup>1</sup> Menghua Li,<sup>1</sup> Qi Liu,<sup>1</sup> Sheng Zhang,<sup>1</sup> Yuan-Qing Xu,<sup>1</sup> Di Wu,<sup>\*,2</sup> Youzhi Xu<sup>\*,1</sup>

<sup>1</sup>College of Chemistry and Molecular Sciences, Henan University, Kaifeng 475004, P. R. China. E-mail: youzhixu@henu.edu.cn

<sup>2</sup>School of Public Health, Zhengzhou University, Zhengzhou 450001, P. R. China. E-mail: wudi22@zzu.edu.cn

<sup>3</sup>School of Chemistry, Zhengzhou University, Zhengzhou 450001, P. R. China.

**Abstract:** The topologically intriguing multimacrocyclic architecture is endowed with distinct physical and chemical properties. The synthesis of hybrid macrocycles combining crown ethers and cycloparaphenylenes (CPPs) presents a promising strategy for developing multifunctional supramolecular systems. Herein, we first report the precise construction of a series of crown ether-CPP hybrid multimacrocycles with enhanced photophysical properties and diverse host-guest interactions. Notably, the trimacrocyclic hybrid adopts a molecular tweezer-like conformation, leading to a five-fold increase in fullerene binding affinity compared to the bismacrocycle. Additionally, the bismacrocycle exhibits significant cytotoxicity against cancer cell lines at low concentrations and enables fluorescence-based detection of inflammatory responses, highlighting its potential for biosensing applications. These findings underscore the versatility of crown ether-CPP hybrid macrocycles in supramolecular chemistry and biochemistry, offering new avenues for the design of functional nanomaterials.

## Introduction

In the realm of supramolecular chemistry, the synthesis and exploration of innovative macrocycles play a pivotal role in advancing materials suitable for applications in drug delivery, catalysis, sensing, and various other fields.<sup>1</sup> Cycloparaphenylenes (CPPs) represent a unique class of  $\pi$ -conjugated macrocycles, distinguished by their strained structure and size-dependent chemical<sup>2</sup> and photophysical properties<sup>3</sup>. These intriguing molecules have attracted considerable attention from researchers in the fields of chemistry and materials science.<sup>4</sup> Recent studies have highlighted the

fascinating properties of topologically unique multi-macrocycles, which exhibit behavior distinct from that of monocyclic structures (Figure 1a).<sup>5</sup> For instance, Du et al. reported CPP-based bismacrocycles that exhibit dual-emission behavior, characterized by tunable aggregation-induced emission and enhanced chiroptical properties.<sup>6</sup> Similarly, Yam and Jiang have independently synthesized rigid and heterotopic bismacrocycles combining CPP and pillar[5]arene, showcasing remarkable luminescent and host-guest recognition properties (Figure 1b).<sup>7</sup>

Crown ethers as an intriguing class of macrocycles with flexible skeleton, renowned for their ability to selectively bind metal cations through coordination interactions and adeptly fabricate mechanically interlocked molecules (MIMs) via hydrogen bonding.<sup>8</sup> This synergy of properties offers exciting opportunities for innovative molecular designs. For example, we recently have reported the synthesis of a rare hetero[3]catenane using a ring-in-ring assembly strategy, incorporating unaltered [12]CPP, 24-crown-8 and a dibenzylammonium macrocycle (Figure 1b).<sup>9</sup> To further explore the potential of the hybrids of CPPs and crown ethers. Herein, we present the synthesis of hybrid bis- and trimacrocycles combining CPPs and crown ethers. We then investigated their supramolecular properties. Additionally, we conducted cell imaging and in vitro antitumor activity studies to evaluate their potential for biological applications.

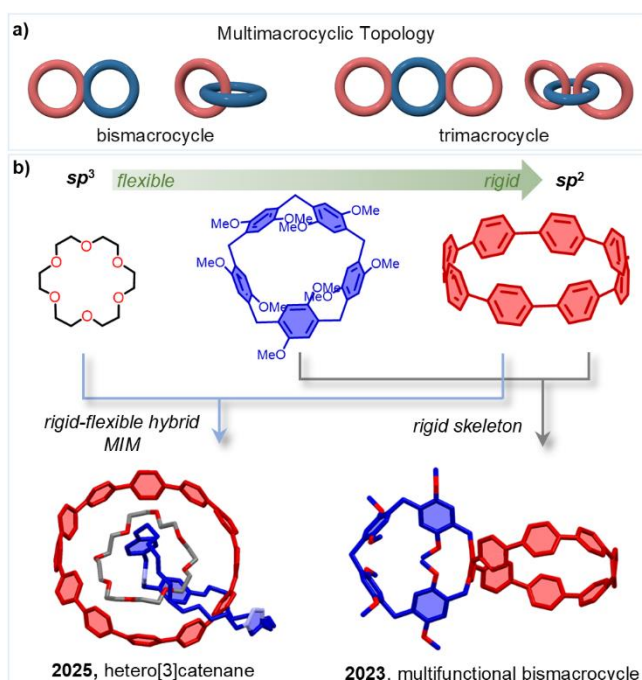
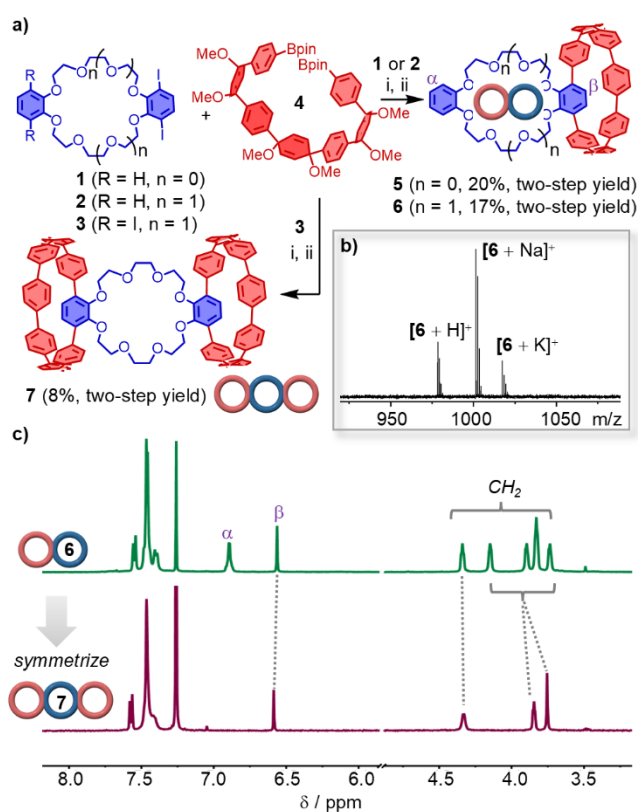


**Figure 1.** a) Illustration of two types of multimacrocyclic topology. b) Selected examples of CPP-hybrid multimacrocycles.

## Result and Discussion

**Synthesis and Characterization.** The pivotal intermediates for the synthesis of bis- and trimacrocycles are outlined in Scheme 1. The hoop-shaped multimacrocycles **5**–**7**, varying in diameter, were successfully synthesized via Suzuki–Miyaura cross-coupling ([dppf Pd G<sub>4</sub>], K<sub>3</sub>PO<sub>4</sub>, 1,4-dioxane–H<sub>2</sub>O, 85 °C, 24 h) between iodinated dibenzo-crown ethers **1**–**3** and diboronate **4**, followed by reductive aromatization (sodium naphthalenide, THF, –78 °C, 2 h). The [8]CPP-based bismacrocycles **5** and **6**, incorporating 18-crown-6 and 24-crown-8, were obtained in with two-step yield of of 20% and 17%, respectively. Using the same approach, the 24-crown-8-bridged trimacrocycle **7** was synthesized with a two-step yield of 8%.

These multimacrocycles were fully characterized by NMR spectroscopy and high-resolution mass spectrometry (HRMS) after standard workup and purification. The crown ether units within the macrocyclic backbone facilitated clear detection of sodium and potassium ion association in the mass spectra (Scheme 1b). Compared to bismacrocycle **6**, trimacrocycle **7** features two identical [8]CPP units flanking the dibenzo-24-crown-8 core, enhancing molecular symmetry, as confirmed by its <sup>1</sup>H NMR spectrum (Scheme 1c).



**Scheme 1.** Synthesis of crown ether-cycloparaphenylene hybrids. a) represent the key synthetic procedures. Reaction conditions: i) [dppf Pd G<sub>4</sub>], K<sub>3</sub>PO<sub>4</sub>, 1,4-dioxane–H<sub>2</sub>O,

85 °C, 24 h. ii) sodium naphthalenide, THF, -78 °C, 2 h. b) The HRMS-ESI of **6**. c) Partial <sup>1</sup>H NMR spectra (CDCl<sub>3</sub>, 298 K, 500 MHz) of **6** and **7**.

Single crystals of **6** were prepared by slow diffusion of diisopropyl ether into toluene solution. As shown in Figure 2 (left), the structure of **6** can be recognized as an integration of the two classic macrocycles, dibenzo-24-crown-8 and [8]CPP. The two independent cavities do not overlap with each other, the distance between the two phenyl rings of dibenzo-24-crown-8 and the diameter of [8]CPP are calculated to be 10.5 Å and 10.4 Å, respectively. Then, we dissolved equimolar amounts of compounds **6** and KPF<sub>6</sub> in a 1:1 CHCl<sub>3</sub>-MeOH solution and obtained single crystals of the metal complex **6**⊃K<sup>+</sup> through slow evaporation of the CHCl<sub>3</sub>. Analyzing the X-ray crystal structure of complex **6**⊃K<sup>+</sup>, we can see that the 24-crown-8 ring tightly encapsulates the potassium ion by folding, primarily via multiple electrostatic interactions, the average distance of O...K is 2.5 Å (Figure 2, right). Due to the introduction of the 24-crown-8 ring, [8]CPP no longer presents ordered columnar packing,<sup>10</sup> but a random packing with no apparent supramolecular interactions between the complex molecules was found in the solid state (Figure S1 and S2). This also leads to **6** having better solubility in organic solvents.

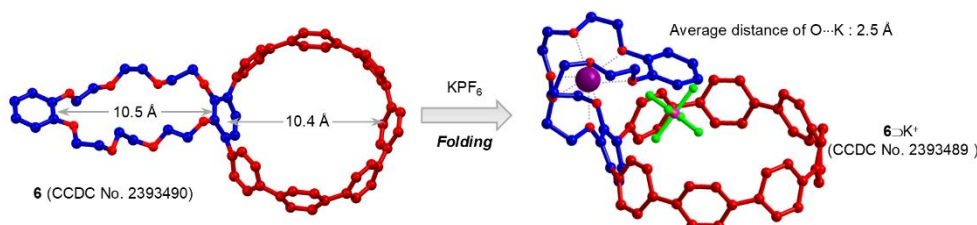


**Figure 2.** X-ray crystal structure of **6** and the complex of **6**⊃K<sup>+</sup>.

**Photophysical Properties.** The absorption spectra of multimacrocycles **6** and **7** closely resemble that of [8]CPP, exhibiting a primary absorption maximum around 335 nm and a shoulder near 400 nm, attributed to the HOMO → LUMO transition. The molar extinction coefficient ( $\epsilon$ ) at 335 nm for **6** ( $8.5 \times 10^4 \text{ M}^{-1} \text{ cm}^{-1}$ ) is comparable to that of [8]CPP, whereas **7** ( $1.3 \times 10^5 \text{ M}^{-1} \text{ cm}^{-1}$ ) exhibits approximately 1.5 times higher absorption. This increase suggests that the two CPP units in **7** behave as independent chromophores, consistent with Beer's Law, although possible excitonic coupling effects cannot be ruled out.

In dichloromethane at 298 K, **6** and **7** display fluorescence emission bands centered at 525 nm and 530 nm, respectively, upon excitation at 340 nm (Figure 3a). Compared to [8]CPP, these multimacrocycles exhibit a slight blue shift, which may arise from

subtle structural distortions induced by the crown ether ring. Such distortions could slightly reduce effective  $\pi$ -conjugation, thereby increasing the energy gap between the excited and ground states. More notably, their fluorescence quantum yields ( $\Phi = 0.58$  for **6**, 0.60 for **7**) are significantly higher than that of [8]CPP ( $\Phi = 0.10$ )<sup>3</sup>, indicating a strong enhancement in radiative emission efficiency. The fluorescence enhancement can be attributed to multiple factors. First, orbital symmetry breaking in the CPP backbone may increase the transition dipole moment, thereby enhancing radiative decay rates (Figure 3b).<sup>11</sup> Second, the introduction of crown ether moieties may impose structural rigidity, reducing non-radiative relaxation pathways such as intramolecular rotations or vibrations. Time-resolved fluorescence measurements reveal that the fluorescence lifetimes of **6** (2.8 ns) and **7** (4.3 ns) are comparable to that of [8]CPP, suggesting that the increased fluorescence quantum yield is primarily due to suppression of non-radiative decay rather than an intrinsic increase in excited-state lifetime. In the solid state, **6** and **7** maintain  $\Phi$  values of 14% and 18%, respectively, despite the potential for aggregation-caused quenching (ACQ). This suggests that the presence of crown ether substituents helps mitigate intermolecular  $\pi$ - $\pi$  stacking, likely by introducing steric hindrance and restricting molecular aggregation.

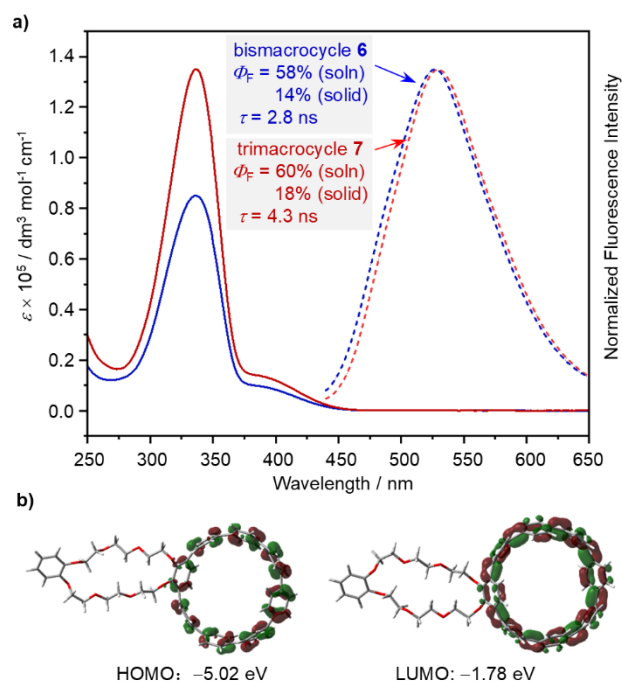


**Figure 3.** a) UV-Vis absorbance (solid lines) and fluorescence (dashed lines) spectra for **6** and **7** (conc.  $5.0 \times 10^{-6}$  M in dichloromethane). b) Frontier molecular orbitals of **6** calculated at the B3LYP/6-31G(d) level of theory (isovalue 0.03).

**Guest Recognition.** Analysis of the X-ray crystal structure of **6** revealed that the flexible crown ether backbone adopts a folded conformation. This structural feature led us to hypothesize that trimacrocyclic **7** might serve as an effective host for fullerene recognition.<sup>12</sup> While [10]CPP is well known for encapsulating C<sub>60</sub> via strong π–π interactions, the smaller size of [8]CPP generally results in weaker binding. Given the structural modifications introduced in **7**, we sought to evaluate its binding properties toward C<sub>60</sub> through fluorescence quenching titrations in toluene.

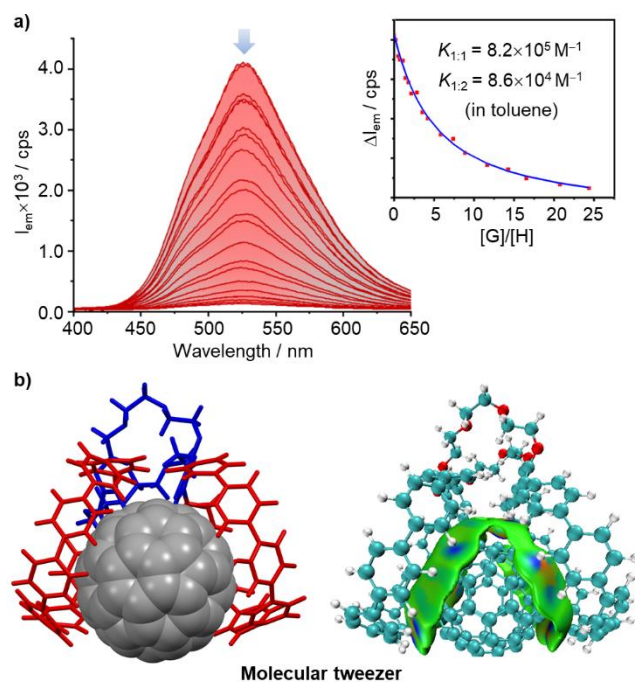


**Figure 4.** a) Fluorescence titrations between **7** (conc.  $1.5 \times 10^{-6} \text{ M}^{-1}$ ) and C<sub>60</sub> in toluene. Association constants were obtained by fitting the data according to a 1:2 (host : guest) stoichiometric model. b) Optimized geometry of **7**⊃C<sub>60</sub> obtained by DFT calculations at B3LYP/6-31G(d) level of theory. IGM analyses of the complex of **7**⊃C<sub>60</sub> ( $\delta g_{\text{inter}}=0.003$ )

The binding study revealed that **6**⊃C<sub>60</sub> forms with an association constant ( $K_A = 1.5 \times 10^{-5} \text{ M}^{-1}$ , Figure S3), which is significantly lower than [10]CPP⊃C<sub>60</sub> ( $3.6 \times 10^{-6} \text{ M}^{-1}$ )<sup>13</sup> but higher than unmodified [8]CPP, likely due to additional dispersion interactions introduced by the crown ether side chains. In contrast, titration experiments between **7** and C<sub>60</sub> exhibited a 1:2 (host : guest) binding equilibrium, with the first binding event showing a much higher association constant ( $K_{1,1} = 8.5 \times 10^{-5} \text{ M}^{-1}$ , Figure S4) compared to **6**⊃C<sub>60</sub>.<sup>14</sup> This suggests that **7** adopts a molecular tweezer-like conformation,<sup>15</sup> where its two CPP units cooperatively encapsulate the fullerene, significantly enhancing its binding affinity. The second binding event occurs with a weaker association constant, likely due to steric hindrance and reduced π–π

interactions when two fullerenes bind to a single host. DFT-optimized structures confirm that C<sub>60</sub> sits symmetrically within the cavity of **7**, stabilized primarily by dispersion forces between the  $\pi$ -conjugated CPP units and the fullerene surface. Independent Gradient Model (IGM) analysis further highlights strong non-covalent interactions in the **7**⊃C<sub>60</sub> complex, reinforcing the enhanced binding affinity observed experimentally.

**Biological Application Evaluation.** Incorporating polar side-chain functionalization into the CPP ring may enhance the macrocycles' utility in biosensing and bioimaging applications.<sup>16</sup> Cell imaging and in vitro antitumor activity studies were performed to evaluate the biological potential of the bismacrocycle **5**. Fluorescence imaging with the HeLa cervical cancer cell line was conducted to assess the bismacrocycle's cellular uptake. After 90 minutes of incubation, weak green fluorescence was observed within the cells, indicating successful penetration of the cell membrane (Figure 5a, A–C). Lipopolysaccharide (LPS), a well-known inflammatory stimulus, induces reactive oxygen species (ROS) production in cells, increasing cytoplasmic viscosity and promoting inflammation.<sup>17</sup> When cells were pretreated with LPS (1  $\mu$ g/mL) for 30 minutes before exposure to the bismacrocycle **5**, a marked increase in fluorescence intensity was observed (Figure 5a, D and E). This enhancement was significantly greater than that in the control group (Figure 5b), suggesting the bismacrocycle's potential for identifying and distinguishing inflammatory cells. The observed increase in fluorescence after LPS pretreatment may be attributed to changes in cellular viscosity, which could facilitate the radiative transition of the compound in inflammatory cells.<sup>18</sup> This finding is important, as it highlights the bismacrocycle's ability to detect and monitor inflammatory responses within cells.

Next, the cytotoxicity of the compound was evaluated in HeLa, H520 (lung cancer), and BEAS-2B (normal lung epithelial) cells using the MTT assay. As shown in Figure 5c, the bismacrocycle **5** exhibited significant cytotoxicity across all cell lines at a minimal concentration of 3  $\mu$ M after 24 hours of incubation. The half-maximal inhibitory concentration (IC<sub>50</sub>) values for HeLa, H520, and BEAS-2B cells were determined to be 3.700, 2.813, and 2.778  $\mu$ M, respectively (Figure 5d). These relatively low IC<sub>50</sub> values underscore the bismacrocycle's potent antitumor activity, which has not been previously reported in the literature.

The bismacrocycle's potent cytotoxicity at low concentrations, with IC<sub>50</sub> values notably lower than those of comparable nanohoops, suggests a superior therapeutic index and

emphasizes its potential as an effective anticancer agent. This is particularly significant given the growing demand for drugs with high potency. Collectively, these findings lay a strong foundation for advancing the compound as a novel imaging agent and anticancer therapeutic, with promising applications in the imaging and treatment of various cancer types.

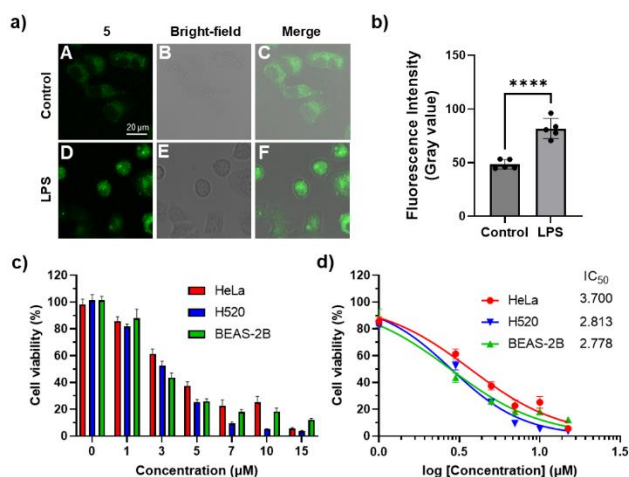


**Figure 5.** a) Confocal fluorescence imaging of HeLa cells. Control groups (A–C): the cells were incubated with **5** for 90 minutes. LPS groups (D and E): The cells were pretreated with LPS (1 μg/mL) for 30 minutes before incubating with **5**.  $\lambda_{\text{ex}} = 405$  nm,  $\lambda_{\text{em}} = 500\text{--}600$  nm. b) Comparison of the fluorescence intensity of the cells in (A) and (D). Data are expressed as the Mean  $\pm$  SD,  $n = 5$ . Statistical significance is denoted by \*\*\*\* ( $p < 0.0001$ ). c) Cell viability and (d) inhibition rates of HeLa, H520, and BEAS-2b cells with different concentrations of the Compound (0, 1, 3, 5, 7, 10, and 15 μM). Data are expressed as Mean  $\pm$  SD,  $n = 3$ .

## Conclusion

In this study, we have successfully designed and synthesized a series of crown ether-CPP hybrid multimacrocycles and explored their supramolecular properties, photophysical behavior, and biological applications. The integration of crown ethers into the CPP framework not only improves solubility and enhances fluorescence quantum yield but also introduces new binding sites that facilitate selective host-guest interactions. Notably, the trimacrocyclic hybrid adopts a molecular tweezer-like conformation, leading to a five-fold increase in fullerene binding affinity compared to its bismacrocyclic counterpart. This enhanced host-guest recognition behavior, supported by fluorescence quenching titrations and density functional theory (DFT) calculations, provides new insights into the design of high-affinity supramolecular receptors.

The biological evaluation of these hybrid macrocycles further underscores their potential for biomedical applications. The bismacrocycle exhibits significant cytotoxicity against cancer cell lines at micromolar concentrations, with IC<sub>50</sub> values lower than those of comparable nano hoops, highlighting its promise as a novel anticancer agent. Moreover, its fluorescence-based detection of inflammatory responses suggests potential applications in biosensing and imaging. These findings collectively demonstrate that crown ether-CPP hybrids represent a new class of multifunctional macrocycles with broad applicability in supramolecular chemistry<sup>19</sup> and biochemistry<sup>20</sup>.

### Acknowledgements

Y.X. acknowledges funding from the National Natural Science Foundation of China (22471060 and 22201064) and The Joint Fund of Henan Provincial Science and Technology Research and Development Plan (235200810074). D.W. acknowledges the Key Scientific Research Project of Colleges and Universities in Henan Province (24A330005).

**Keywords:** Cycloparaphenylene; Crown Ether; Molecular Tweezer; Multimacrocycle; Fullerene Binding

### References:

1. (a) T. Ogoshi, T. A. Yamagishi and Y. Nakamoto, *Chem. Rev.*, 2016, **116**, 7937–8002. (b) X. Chang, Y. Xu and M. von Delius, *Chem. Soc. Rev.*, 2024, **53**, 47–83. (c) X.-N. Han, Y. Han and C.-F. Chen, *Chem. Soc. Rev.*, 2023, **52**, 3265–3298. (d) Y. Yu, Y. Hu, C. Ning, W. Shi, A. Yang, Y. Zhao, Z.-Y. Cao, Y. Xu and P. Du, *Angew. Chem. Int. Ed.*, 2024, **63**, e202407034.
2. (a) T. D. Clayton, J. M. Fehr, T. W. Price, L. N. Zakharov and R. Jasti, *J. Am. Chem. Soc.* 2024, **146**, 30607–30614. (b) Y. Xu, M.-Yi Leung, L. Yan, Z. Chen, P. Li, Y.-H. Cheng, M. H.-Y. Chan and V. W.-W. Yam, *J. Am. Chem. Soc.*, 2024, **146**, 13226–13235. (c) W. Shi, Y. Zhao and Y. Xu, *Trends Chem.*, 2025, **7**, 1–2.
3. E. R. Darzi and R. Jasti, *Chem. Soc. Rev.*, 2015, **44**, 6401–6410.
4. (a) Y. Li, H. Kono, T. Maekawa, Y. Segawa, A. Yagi and K. Itami, *Acc. Mater. Res.*, 2021, **2**, 681–691. (b) J. Malinčič, S. Gaikwad, J. P. Mora-Fuentes, M.-A. Boillat, A. Prescimone, D. Häussinger, A. G. Campaña and T. Šolomek, *Angew. Chem. Int. Ed.*, 2022, **61**, e202208591. (c) M. Hermann, D. Wassy and B.

- Esser, *Angew. Chem. Int. Ed.*, 2021, **60**, 15743–15766. (4) A. Stergiou, J. Rio, J. H. Griwatz, D. Arcon, H. A. Wegner, C. Ewels and N. Tagmatarchis, *Angew. Chem. Int. Ed.*, 2019, **58**, 17745–17750.
5. (a) X.-L. Chen, S.-Q. Yu, X.-H. Huang and H.-Y. Gong, *Molecules* 2023, **28**, 6043. (b) Y. Zhang, D. Yang, S. H. Pun, H. Chen and Q. Miao, *Precis. Chem.* 2023, **1**, 107–111. (c) J. He, M.-H. Yu, Z. Lian, Y.-Q. Fan, S.-Z. Guo, X.-N. Li, Y. Wang, W.-G. Wang, Z.-Y. Cheng and H. Jiang, *Chem. Sci.*, 2023, **14**, 4426. (d) X. Zhang, Y. Xu and P. Du, *Acc. Mater. Res.*, 2025, DOI: 10.1021/accountsmr.4c00338. (e) G. Li, L.-L. Mao, J.-N. Gao, X. Shi, Z.-Y. Huo, J. Yang, W. Zhou, H. Li, H.-B. Yang, C.-H. Tung, L.-Z. Wu and H. Cong, *Angew. Chem. Int. Ed.*, 2025, **64**, e202419435. (f) Y. Yang, O. Blacque, S. Sato and M. Juriček, *Angew. Chem. Int. Ed.*, 2021, **60**, 13529–13535. (g) L. Ren, Y. Han, X. Hou, Y. Zou, T. Jiao and J. Wu, *CCS Chem.*, 2024, **6**, 2758–2769. (h) X.-W. Chen, Q.-S. Deng, B.-H. Zheng, J.-F. Xing, H.-R. Pan, X.-J. Zhao, and Y.-Z. Tan, *J. Am. Chem. Soc.* 2024, **146**, 31665–31670. (i) K. Li, S. Yoshida, R. Yakushiji, X. Liu, C. Ge, Z. Xu, Y. Ni, X. Ma, J. Wu, S. Sato and Z. Sun, *Chem. Sci.* 2024, **15**, 18832–18839.
6. X. Zhang, H. Liu, G. Zhuang, S. Yang and P. Du, *Nat. Commun.*, 2022, **13**, 3543.
7. (a) Y. Xu, F. Steudel, M. Leung, B. Xia, M. von Delius and V. W-W Yam, *Angew. Chem. Int. Ed.* **2023**, **62**, e202302978. (b) Y. Fan, S. Fan, L. Liu, S. Guo, J. He, X. Li, Z. Lian, W. Guo, X. Chen, Y. Wang and H. Jiang, *Chem. Sci.*, 2023, **14**, 11121–11130. (c) Y. Zhou, G. Zhuang and P. Du, *Chin. Chem. Lett.*, 2024, **35**, 108593.
8. (a) J. E. M. Lewis, P. D. Beer, S. J. Loeb, S. M. Goldup, *Chem. Soc. Rev.* 2017, **46**, 2577–2591. (b) L. Chen, X. Sheng, G. Li and F. Huang, *Chem. Soc. Rev.*, 2022, **51**, 7046–7065. (c) N. H. Evans and P. D. Beer, *Chem. Soc. Rev.* 2014, **43**, 4658–4683. (d) A. Goswami, S. Saha, P. K. Biswas and M. Schmittel, *Chem. Rev.* 2019, **120**, 125–199.
9. W. Shi, Y. Hu, L. Leanza, Y. Shchukin, P. A. Hoffmann, M. Li, C. Ning, Z.-Y. Cao, Y. -Q. Xu, P. Du, M. von Delius, G. M. Pavan and Y. Xu, *Angew. Chem. Int. Ed.*, 2025, **64**, e202421459.
10. J. Xia, J. W. Bacon and R. Jasti, *Chem. Sci.*, 2012, **3**, 3018–3021.
11. T. C. Lovell, C. E. Colwell, L. N. Zakharov and R. Jasti, *Chem. Sci.*, 2019, **10**, 3786–3790.
12. (a) Y. Xu and M. von Delius, *Angew. Chem. Int. Ed.* 2020, **59**, 559–573. (b) C. García-Simón, M. Costas and X. Ribas, *Chem. Soc. Rev.*, 2016, **45**, 40–62.
13. T. Iwamoto, Y. Watanabe, T. Sadahiro, T. Haino, S. Yamago, *Angew. Chem. Int.*

*Ed.* 2011, **50**, 8342–8344.

14. (a) A. Sacristan-Martin, H. Barbero, S. Ferrero, D. Miguel, R. Garcia-Rodriguez and C. M. Alvarez, *Chem. Commun.*, 2021, **57**, 11013–11016. (b) B. Scholz, A. S. Oshchepkov, O. Papaianina, C. Ruppenstein, V. A. Akhmetov, D. I. Sharapa, K. Y. Amsharov and M. E. Pérez-Ojeda, *Chem. – Eur. J.*, 2023, **29**, e202302778. (c) M. S. Mirzaei, S. Mirzaei, V. M. E. Castro, C. Lawrence and R. H. Sánchez, *Chem. Commun.*, 2024, **60**, 14236–14239.
15. <http://supramolecular.org>
16. (a) K. Günther, H. Kono, H. Shudo, D. Shimizu, R. Isoda, M. Nakamura, A. Yagi, K. Amaike and K. Itami, *Angew. Chem. Int. Ed.* 2025, **64**, e202414645. (b) B. M. White, Y. Zhao, T. E. Kawashima, B. P. Branchaud, M. D. Pluth, R. Jasti, *ACS Cent. Sci.*, 2018, **4**, 1173–1178.
17. (a) Y. Zhang, Z. Li, W. Hu and Z. Liu, *Anal. Chem.* 2019, **91**, 10302-10309. (b) Y.-Y. Li, J.-L. Hu, J.-R. Wu, Y.-R. Wang, A.-H. Zhang, Y.-W. Tan, Y.-J. Shang, T. Liang, M. Li, Y.-L. Meng and Y.-F. Kang, *Biosens. Bioelectron.*, 2024, **254**, 116233.
18. (a) S. Feng, S. Gong, Z. Zheng and G. Feng, *Sensor. Actuat. B-Chem.* 2022, **351**, 130940. (b) W.-N. Wu, Y.-F. Song, X.-L. Zhao, Y. Wang, Y.-C. Fan, Z.-H. Xu and T. D. James, *Chem. Eng. J.*, 2023, **464**, 142553.
19. (a) Q. Chen and K. Zhu, *Chem. Soc. Rev.*, 2024, **53**, 5677–5703. (b) Z. Zhang, J. Zhao and X. Yan, *Acc. Chem. Res.* 2024, **57**, 992–1006.
20. K. Chinner, N. Grabicki, R. Hamaguchi, M. Ikeguchi, K. Kinbara, S. Toyoda, K. Sato and O. Dumele, *Chem. Sci.* 2024, **15**, 16367–16376.

## TOC:

